RRI-GBT Multi-Band Receiver: Motivation, Design & Development

Yogesh Maan[1,2], Avinash A. Deshpande[1], Vinutha Chandrashekar[1], Jayanth Chennamangalam[1,3], K. B. Raghavendra Rao[1], R. Somashekar[1], Gary Anderson[4], M. S. Ezhilarasi[1], S. Sujatha[1], S. Kasturi[1], P. Sandhya[1], Jonah Bauserman[4], R. Duraichelvan[1], Shahram Amiri[1,8], H. A. Aswathappa[1], Indrajit V. Barve[5], G. Sarabagopalan[1], H. M. Ananda[1], Carla Beaudet[4], Marty Bloss[4], Deepa B. Dhamnekar[1], Dennis Egan[4], John Ford[4], S. Krishnamurthy[1], Nikhil Mehta[1,6], Anthony H. Minter[4], H. N. Nagaraja[1], M. Narayanaswamy[1], Karen O'Neil[4], Wasim Raja[1], Harshad Sahasrabudhe[1,7], Amy Shelton[4], K. S. Srivani[1], H. V. Venugopal[1], Salna T. Viswanathan[1]

ABSTRACT

We report the design and development of a self-contained multi-band receiver (MBR) system, intended for use with a single large aperture to facilitate sensitive & high time-resolution observations simultaneously in 10 discrete frequency bands sampling a wide spectral span (100-1500 MHz) in a nearly log-periodic fashion. The development of this system was primarily motivated by need for tomographic studies of pulsar polar emission regions. Although the system design is optimized for the primary goal, it is also suited for several other interesting astronomical investigations. The system consists of a dual-polarization multi-band feed (with discrete responses corresponding to the 10 bands pre-selected as relatively RFI-free), a common wide-band RF front-end, and independent back-end receiver chains for the 10 individual sub-bands. The raw voltage time-sequences corresponding to 16 MHz bandwidth each for the two linear polarization channels

[1]Raman Research Institute, Bangalore, India

[2]Joint Astronomy Programme, Indian Institute of Science, Bangalore, India

[3]Department of Physics, West Virginia University, PO Box 6315, Morgantown, WV, USA

[4]National Radio Astronomy Observatory, PO Box 2, Green Bank, WV, USA

[5]Indian Institute of Astrophysics, Bangalore, India

[6]Department of Electrical Engineering, The Pennsylvania State University, Pennsylvania, USA

[7]Department of Physics, Purdue University, West Lafayette, IN, USA

[8]School of Physics & Astronomy, University of Manchester, Oxford Road, Manchester, UK

and the 10 bands, are recorded at the Nyquist rate simultaneously. We present the preliminary results from the tests and pulsar observations carried out with the Green Bank Telescope using this receiver. The system performance implied by these results, and possible improvements are also briefly discussed.

Subject headings: Instrumentation: polarimeters – Instrumentation: miscellaneous – Methods: observational – pulsars: general – pulsars: individual (B0329+54) – pulsars: individual (B0809+74)

1. Introduction

Even after several decades of pulsar studies, we remain far from being able to relate the puzzling rich details exhibited by pulsars to the physical processes responsible for the observed radio emission. While the average pulse profile with polarization information reveals the viewing geometry (Radhakrishnan & Cooke 1969) and gives some clues about the possible emission mechanisms (for example, see Rankin 1983, and other papers in the same series), the fluctuations from pulse to pulse seem to be more crucial and promising in probing the underlying physical processes (see, for example Drake & Craft 1968; Backer 1973; Deshpande & Rankin 1999). Over the past decade, studies of such fluctuations in pulsar signals suggest that plasma processes responsible for pulsar emission may be organized into a system of columns seeded by a well-defined pattern of "spark" discharges in the acceleration region and undergoing steady circulation around the magnetic axis. Estimation of this circulation time, and hence "cartographic" mapping of the observed emission to a system of emission columns has been possible so far only for a limited number of pulsars, and the important factors determining such configurations and the pattern circulation are yet to be fully understood. Further, any possible connection between the profile/polarization mode changes, as well as nulling, observed in several pulsars and the circulating patterns also needs careful investigations. To enable these investigations, ideally, we need full polarimetric data on how the emission columns and their configuration evolves with emission height and time. This demands simultaneous single-pulse observations across a wide frequency range implied by the so called radius-to-frequency mapping; with the high frequency emission originating close to the star surface, and regions of lower frequency emission progressively farther away. However, most of the available observations are made at a time over a narrow spectral range, thus sampling the details only in a slice of the emission cone. The limitation largely comes from considerations of radio frequency interference (RFI), even if wide-band systems were to be available. The need for a setup enabling multi-frequency observations, essential to sample the polar magnetosphere at various heights simultaneously, can not be overstated. With

such observations, polar emission mapping at a number of frequencies would not only allow "tomography" of the polar emission region (see an illustration in figure 1), but also might provide much needed clues about generation of sub-beam patterns, associated polarization and their evolution across the magnetosphere.

While in principle, simultaneous multi-frequency observations can be carried out using many telescopes simultaneously, practical difficulties in this approach are numerous. Apart from inherent complexities in coordinating/scheduling several telescopes at different geographical locations, their available setups might have undesirable differences in, say, hour angle coverage, aperture shape & filling factor, polarization response, ionospheric contributions, synchronization (time-stamp) accuracy, calibration schemes, sensitivity, RFI-free bands and data formats. A superior alternative which provides the desired simultaneous multi-frequency observations, avoiding all the above complexities, is to have a "self-contained" multi-band system for use with a single large aperture. Such a system would include a suitable feed, broadband front-end, parallel analog & digital receiver pipelines, along with appropriate monitoring, synchronization and data recording systems. It is beneficial to sample the signal voltages in dual polarization at each of the multiple bands, pre-selected to avoid RFI as much as possible.

We present here the design and development of such a self-contained multi-band receiver system (MBR) for use with the Green Bank Telescope (GBT), and describe preliminary results from observations using this setup.

Section 2 below gives a detailed hardware description of the system, section 3 describes the control and monitor module. In section 4, we present the preliminary results from the tests & observations at GBT. We discuss the system performance and possible future developments in the concluding section.

2.   MBR System: Hardware Details

The overall block diagram of the MBR system, designed and developed at the Raman Research Institute (RRI), is shown in Figure 2. The signal path begins with a dual linear polarization multi-band feed sensitive to 10 discrete bands within a spectral span of 100-1600 MHz, followed by appropriate pre-amplification, filtering, up-conversion, transmission over the optical fiber, down-conversion, splitting in to bands of interest, superheterodyning to intermediate frequency (IF), digitization and recording. Below we describe various parts of the MBR system along this signal path.

2.1. Multi-Band Feed

Broadband feeds spanning more than a decade in spectral range are not commonly used in radio astronomy. Not only because their designs are challenging, their utility in practice is severely compromised due to ever increasing RFI from communication signals occupying a large fraction of the radio band at frequencies below 2 GHz. Low level RFI can be detected and excised during post-processing of the recorded data. However, the presence of strong RFI in certain bands not only makes the specific bands unusable, but it may also contaminate the otherwise cleaner regions due to possible non-linear system response at high power levels. It is desirable therefore to reject RFI as early in the signal path as possible. Noting the challenges in designing feeds with uniform performance over a wide-band and the mentioned RFI issue, we have considered a multi-band design with good response only over selected bands to provide preliminary immunity against RFI. As will be described later, the bands with severe RFI are filtered out explicitly soon after the signals from the feed are pre-amplified adequately (so as to minimize the effect of filter insertion losses in the desired band).

For a broadband feed antenna at the prime focus of a parabolic dish, it is important to ensure that the phase center of the feed remains independent of frequency. Also desirable is a good match between the E & H plane responses, while using linear feeds or their combinations to illuminate circular apertures uniformly. In view of these, we find the basic conical arrangement of active elements as in the "Eleven Feed" (Olsson, Kildal & Weinreb 2006) to be most suited for our purpose. In these feeds, log periodic dipole-arrays are arranged in pairs at 45° about the symmetry axis for each one of the two linear polarizations (constraining the apex angle of each of the dipole-arrays to 35°). In the Eleven feed the phase center does not move significantly with frequency, and the spectral response is rather uniform across the design band. Our design differs significantly from that of the Eleven feed specifically in the latter of these two aspects. As shown in Figure 3, we use a plane reflector (ground plane, 1.7 m across) perpendicular to the axis of the conical structure. For each one of the dipoles in the four dipole-arrays, when considered together with its corresponding image, the combined phase center would be at the symmetry point in the plane of the reflector. Extending this picture to two dipoles of a given frequency, corresponding to a pair of dipole arrays for one polarization, it is easy to see that the phase center of the combination will be at the apex of the cone in the reflector plane. More importantly, this would be independent of frequency, and in principle also independent of the opening angle of the cone. Each of the dipole arrays following an approximately log-periodic pattern, consists of a set of resonant dipoles corresponding to the bands of interest, chosen as the relatively RFI-free parts of the wide-band. A number of multi-band feed designs, differing in dipole arrays, their mounting and feed-point connections, were experimented with, keeping the basic conical arrangement

and the ground reflector as mentioned above. Details of a couple of the early designs, and their performances can be found in Maan et al. (2009). The final design of the dipole array (Figure 3) consists of 10 simple half-wave dipoles arranged in a quasi-log-periodic fashion, along with a stub terminating the feed-line past the longest wavelength dipole and an extra shorter dipole past the highest frequency resonant dipole. The dipoles are realized using aluminium tubes and rods at frequencies below and above 300 MHz respectively, with diameters progressively decreasing with wavelength as far as possible. The central feed-line (of length 73.5 cm) consists of a pair of 10 mm aluminium square rods and the stub at its end made of a 10 mm wide, 2 mm thick aluminium strip. The length of the stub was optimized based on a combined criteria of favorable and poor response of the feed-line (modelled as a transmission line with one end shorted) at the desired and the RFI bands respectively. The value obtained from a computer program to search for the optimum length matched well with that assessed from trial & error. The support structure for the dipole arrays (conical section behind the dipoles in Figure 3) is made of fiber glass material, keeping it light-weight but sturdy. The dipoles are secured on this structure with the help of Nylon bolts and the face of the cone is covered with Tecron cloth. The presence of dielectric behind the dipoles does, in principle, affect their performance. Hence, the conical profile was maintained only till the 430 MHz dipole, since the effects at this and lower frequencies are not serious. In the lower part of the structure, the close proximity to (higher frequency) dipoles is avoided by the profile deviating from the conical to a boxy profile at the base. The resonant dipole at the lowest frequency would have been too long to accommodate within the size constraints at the prime focus of the GBT. Hence, a shorter length dipole is used, with its location on the feed-line appropriate to its actual length, thus reducing the overall size of the feed. The feed-line is designed with a characteristic impedance of 50 Ω, and a co-axial cable is directly connected to the feed-points of each of the four dipole arrays. These cables are kept short in length, just enough to reach the pre-amplifiers located immediately below the reflector.

The in-phase combination of the two dipole arrays at angles $\pm45°$ about the feed axis and corresponding to a given linear polarization, provides a good match between the E & H plane beams. For a beam with full width at half power of about 60°, and the half angle of 42° for the GBT dish as seen from its prime focus, the edge taper would be at least -7 dB, before including the inverse square law dependence on the distance from the feed. This would amount to relatively larger spill over than usual, but would illuminate a larger effective collecting area. In comparison, the edge taper inferred from the beam-width, as we will see later, is somewhat larger (in the range -15 dB to -20 dB). Figure 2 (top right panel) shows a typical return-loss profile across the spectrum for one of the dipole array pairs corresponding to one of the polarizations. The feed cross-polarization is measured, both during the feed tests and from observations of bright unpolarized sources, and is found to be at the level of

$-20\,dB$.

2.2. Wide-band RF Front-end

As noted above, each of two dipole-array outputs corresponding to a linear polarization are first amplified separately and then combined in phase. As a wide-band ($\leq$ 2 GHz) low noise amplifier (LNA), we have used a commercially available module of Mini Circuits ZX60-33LN, with a typical gain of around $20\,dB$ and noise-figure less than $1.3\,dB$ over the band of interest. The pre-amplified signals, after the respective pairs are combined, provide dual orthogonal polarization outputs that are passed through a band limiting filter (100-1600 MHz), realized using appropriate combination of low pass and high pass filters. After further nominal amplification, the bands associated with known strong RFI signals (e.g. FM radio signals, TV transmission & mobile communication and those particular to the geographical location of the system; presently GBT) within our primary band are rejected using a cascade of home-made band-reject filters. At this point, since the primary contaminants are removed, larger amplification is possible and needed to carry the signals from feed location to the receiver room. The modules in the receiver room prepare the signal for subsequent transmission to the equipment room via existing optical fiber system. These modules up-convert the RF band of 100-1600 MHz to 2000-3500 MHz, using a local oscillator (LO) of 3.6 GHz. Noting that the band is flipped in this translation, appropriate length RF cable is introduced in the path (in order to use its frequency dependent attenuation characteristics) to at least partly compensate for the effect of gain-slopes introduced in the earlier stages. In the equipment room, the received band is down-converted back to the original RF band of 100-1600 MHz, using an LO again of 3.6 GHz.

2.3. Sub-band Receiver Chains

The wide-band RF signal received in the equipment room is split into 10 fixed sub-bands[1] after adequate amplification in anticipation of the power-divider losses. The bandwidths of the filters separating the different bands varies typically between 20 to 120 MHz, decided based on the RFI situation[2]. The details of the central radio frequency values and the

---

[1] Although the system was originally conceived to provide operation with 8 sub-bands, 2 additional back-end chains built as spares were also made part of the system providing 2 extra sub-bands.

[2] An RFI survey at the observing site was performed primarily around the desired sub-bands, and the nearest available relatively RFI-free regions were selected.

corresponding bandwidths of the 10 RF sub-bands are given in the table in Figure 2. The chosen bands provide nearly log-periodic sampling within the wide-band.

2.3.1. Analog Pipeline

The 10 signals, thus obtained, are processed through very similar high gain chains, each consisting of an amplifier-attenuator combination for RF, a mixer followed by a filter, an amplifier-attenuator combination & another band-defining filter for IF, in that sequence. The LO signal, required for the RF to IF conversion, is generated using a discrete PLL (phase-locked-loop) wherein a VCO (voltage controlled oscillator) is phase-locked to a 10 MHz signal from a rubidium standard, which in turn is disciplined with a 1PPS (pulse per second) derived from the Global Positioning System (GPS). The LO frequency can be selected in steps of 1 MHz, within a range large enough to tune in to any region of the respective RF sub-bands. Care is taken in choice of the IF frequency to ensure that the IF as well as any image band falls outside the respective RF sub-band. Thus, the IF center frequency for most of the chains is 140 MHz while it is 70 MHz for the two lowest RF bands (below 200 MHz). The IF-filters are commercial surface acoustic wave (SAW)-filters of 16 MHz bandwidth, providing a sharp roll-off characteristic and good rejection outside the IF band. The second of the IF-filters is necessary to suppress out-of-band noise-floor contributed by the electronics following the first of the IF-filters. The independent attenuators in the RF and IF sections, which are computer controlled and provide attenuation within 0 to 31 dB in steps of 0.5 dB, are used to adjust the signal level to ensure operation in the linear regime of the chain. The net amplification in the signal path is arranged to be typically in excess of 100 dB so as to provide a suitable level of IF input to the analog-to-digital converter (ADC).

2.3.2. Digital Section

The IF signals for the two polarizations corresponding to a given sub-band, with 16 MHz bandwidth & centered at 140/70 MHz, are digitized directly using harmonic sampling. A low-power, 8-bit dual-channel ADC (AD9288 from Analog Devices) capable of operating at 100 mega samples per second, and with an analog bandwidth of 475 MHz is used for this purpose (see Figure 4), providing high dynamic range[3]. The sampling clock frequency in our case is 33 (or 31.25) MHz for IF bands at 140 (or 70) MHz. The ADC is controlled by a

---

[3]Tests with a CW input at frequency of 16 MHz to characterize the ADC indicated SNR of 32 dB, implying the Effective Number Of Bits (ENOB) to be 5.5 for each of the two channels.

CPLD (Complex Programmable Logic Device; XC9572XL), configured using VHSIC hardware description language (VHDL), where an input clock at twice the sampling frequency is de-multiplexed and fed to the two channels of the ADC. At the start of each acquisition, the clocks are synchronized with respect to 1 PPS signal generated from GPS-disciplined rubidium standard. The dual channel 8-bit samples along with strobe are time multiplexed and passed to the following module.

The digital back-end is realized using a Xilinx-ML506 evaluation board consisting of a Virtex-5 FPGA (field programmable gate array), and a rack-mountable PC. The 8-bit parallel input stream at the rate of about 66 mega-samples per second, representing multiplexed raw voltage samples from the two orthogonal polarization channels, is received and after appropriate packetization the data are transmitted to the PC on a Gigabit Ethernet (GbE) channel. The FPGA firmware for this purpose has been developed in VHDL. The GbE interface logic is realized on the FPGA using the intellectual property (IP) core "Embedded Tri-Mode Ethernet MAC Wrapper v1.3" provided by Xilinx. The basic block diagram of the digital back-end receiver is shown in Figure 4. The on-board FPGA is programmed through a serial port on the PC via a micro-controller. Initialization is performed through a master reset bit generated by control software on the PC. The functionality in the FPGA includes generation of both the sampling clock (66/62.5 MHz, used by ADC) and a 100 MHz clock used for reading the ADC data buffered through a FIFO (First In First Out). These programmable clocks are generated from an input reference clock at 10 MHz (from the already mentioned rubidium standard) using the digital clock manager (DCM) blocks in the FPGA. A GPS-disciplined rubidium-based 1PPS input to the FPGA is used for both, synchronization at the start of the acquisition as well as for its time-stamping. Several pieces of information relevant to receiver settings and acquisition details (sent from the control software on the PC) are decoded, using a separate firmware, before their inclusion in the packet header.

The FPGA logic is designed to transmit the data and header information in packet form, using the user datagram protocol (UDP). Each data packet consists of 42 bytes of protocol header (Ethernet, IP and UDP headers), 32 bytes of MBR header (which contains the identity of the receiver, status information like mode of operation, GPS counter, and packet counter), and 1024 bytes of digitized data (dual-polarization, interleaved), as shown in Figure 5. Any change made in the system settings is reflected instantaneously in the headers associated with the acquired data (i.e. in the data-packet immediately following the change).

3.   MBR System: Software Details

The monitoring & control of the MBR as well as data acquisition are handled by a specially developed software suite. The 10 PCs provide the platform on which the relevant codes are executed in coordination with a master monitoring-and-control (M&C) PC. These 10 PCs, referred to as data acquisition subsystems (DAS), and the M&C PC (or machine) are interconnected through a GbE-switch.

The software that runs on the MBR system is divided into three major components – commands, the M&C daemon, and the DAS daemons, the latter two running on respective machines. Commands may be given either from the M&C machine or from a remote machine connected to it, such as a machine on the GBT network. The M&C daemon acts as a command router – it receives user commands and dispatches them to the relevant DAS machine. The DAS daemon running on a DAS machine receives the commands intended for it, and executes them. It also returns command status information back to the M&C machine. A command is a program that works in two modes – in 'remote mode', the program sends a command string to the M&C daemon, and in 'local mode' (when given on the DAS machine) executes the task it is expected to perform. Commands include control commands and monitoring commands. The general form of a command is '<*command*> <*das-id*> <*parameter*> <*value*>', where <*command*> can be one of three types – 'set', 'get', and 'do'. The first two types are used to set and retrieve system settings, respectively, whereas the third type is used to perform specific tasks, such as triggering data acquisition. A command can be initiated from the GBT observation system either by executing the command binary directly, or by sending the equivalent command string to the M&C daemon over a socket connection. <*das-id*> is a numeric identifier specifying which DAS machine the command is intended for. A value of 0 results in the broadcasting of the command to all the 10 DAS machines. <*parameter*> and <*value*> can be, as the names imply, names of configurable parameters and their possible values. The M&C software system architecture, depicting a sample command flow, is shown in Figure 6. Each of the DAS machines is connected to the digital back-end through a GbE link. When triggered, the data-acquisition program runs on the DAS machines, recording packeted data to the disk. In addition, it sends samples of these data at a significantly reduced packet rate to the M&C machine for monitoring purpose, as described later in this section.

The software based control, using the command structure mentioned above, also facilitates setting of RF/IF attenuation & LO frequency relevant to the analog section, and bit-packing mode & GPS synchronization for the digital back-end. The information about the receiver settings is stored in configuration files on the DAS machines, as well as on the M&C machine, and updated as necessary. Similarly, the control software caters to commands

for initiation & termination of data acquisition, apart from settings specifying duration & mode of acquisition (i.e. with or without monitoring enabled).

The configuration files containing all the up-to-date settings and status information are accessed to query & monitor parameters of interest, without actually having to read from the hardware. The monitoring of data, on the other hand, involves 'sniffing' (i.e. infrequent sampling) 1 packet out of every 1000 received/recorded on the DAS machines, and sending them to the M&C machine. On the M&C machine, the sniffed data received from all the 10 DAS machines are recorded for subsequent monitoring & checks. Checking for the expected pattern in the packet counter values, available in the headers of received packets, serves as a quick diagnostics of acquisition on the respective das machines. Processing of these sniffed data is performed by a separate code and quasi-real-time spectra (in full stokes), as well as total power time-sequences can be monitored. Other tasks that can be performed by this code include estimation and automatic adjustment of the gains of individual receiver chains to equalize the output power levels, a tool often used before the start of acquisition. Spectral scans can also be performed, by stepping through LO settings, to assess system gain and RFI occupancy across the accessible spectral span, for all chains simultaneously.

4. Observations and Preliminary Results

After successful intensive laboratory tests, performance of the MBR system was assessed through preliminary observations, wherein the broad beam of the multi-band feed was slewed across bright astronomical sources. These tests were conducted at the RRI field station – Gauribidanur observatory – which provided a relatively RFI free environment. To test the system including its use with a shaped reflector, the feed was installed at the prime focus of one of the GMRT (Giant Meter-wave Radio Telescope) dishes (see Maan et al. 2009, for details). Through the more sensitive measurements made possible by the large collecting area of the dish, the performance of the feed and the system as a whole was characterized in terms of aperture & beam efficiencies, system temperature, etc. These tests provided valuable feedback which prompted improvements in the feed design and in the filtering strategy in the front-end.

After these revisions, the system was moved to Green Bank in May, 2009. A standard GBT receiver-box (used at its prime focus) was made available to house the MBR front-end as well as to attach the multi-band feed. After the system was fully installed, test observations were conducted on a few bright continuum sources. These resulted in measurements of the beam patterns as well as helped in deciding the optimum location of the feed based on a focus scan. Attenuation/gain adjustments necessary to operate within linear regime of the

optical fiber system at GBT were incorporated, and using spectral scans, regions of better sensitivity were identified for each of the bands. The beam-widths (full widths at half power) corresponding to the two polarizations, estimated from slew-scans across the bright radio source Cas-A, are shown as a function of wavelength in Figure 7. The scan data, obtained simultaneously in all the 10 bands, are as shown in the panel labelled "On-the-fly Temporal Monitoring" in Figure 2. As desired, the illumination of the GBT dish by the multi-band feed appears uniform across frequency (reflected by the goodness of the linear fit). If interpreted assuming Gaussian illumination, the illumination efficiency is about 75%. Given possible differences in the E & H plane beams, and the different diameters of the GBT dish in the orthogonal directions (i.e. 100 & 110 meters), the implied edge-taper would be in the range -15 dB to -20 dB.

After the above tests, about 20 hours of observations were carried out on a number of bright pulsars, along with short duration pointings at Cas-A, Cygnus-A and Crab as flux calibrators. The results from these data (enabling investigation of single pulse fluctuations over multiple bands simultaneously) and the related implications for the underlying sub-beam pattern & its evolution over emission height, etc., will be reported elsewhere. However, in this paper we conclude with presentation of illustrative examples of the type of data obtained with this MBR system. Figure 8 shows the phase-aligned average profiles of the pulsar B0329+54 observed in 9 bands of the MBR (the 10th band data were unavailable due to an unfortunate computer crash). A sample of raw dynamic spectra in the corresponding bands, illustrating typical data quality (including RFI contamination) across the respective bands, is shown in Figure 9. From several pulsars observed to study drifting sub-pulses, we use the B0809+74 observation to illustrate construction of a tomograph. In this case, the secondary periodicity (associated with sub-pulse drift) is ~ 11 spin periods. In each sub-band, the emission pattern is mapped using cartographic transform. While the details of analysis on this pulsar and the assumed tertiary periodicity would be discussed elsewhere, here we present a preliminary tomograph of the polar emission region of this pulsar in Figure 10, using data in the lowest 4 frequency bands having adequate signal-to-noise ratio.

5. Discussion and Conclusions

The examples shown in previous section have illustrated the quality and the types of data obtained in simultaneous multi-frequency observations facilitated by the MBR. The efficiency of illumination of the GBT reflector by our feed appears quite uniform across the 10 bands, and our focus scans taken on strong continuum sources during the commissioning tests indicate the feed phase-center to be independent of frequency. Although the feed

performance is as desired in these aspects, we find significant loss of sensitivity at the higher frequency bands in general, and at the 1200 & 1450 MHz bands in particular. Implicit in our feed design is the requirement that the two dipole arrays corresponding to a given linear polarization are phased correctly, particularly at the frequencies of interest. This requires matching of spectral responses between the two arrays, and any mismatch in them would cause improper phasing (since phase may vary rapidly about the respective resonant frequencies), and consequently significant de-phasing across the primary reflector that the feed illuminates. In practice, the desired match is difficult to ensure at higher frequencies where small differences in the mechanical structure and feed-point connections can cause noticeable mismatch. Such mismatch, if any, would manifest in distortion of the resultant beam-shape. Except in one of the bands (i.e. at 630 MHz, and in one of the polarizations, as seen in Figure 2), such distortion is not apparent, indicating reasonable match within the array pair in all other bands, including those at higher frequencies. A closer look at the beam width estimates reveals that they deviate significantly from the mean trend at the two shortest wavelengths (Figure 7), possibly implying the illuminated area to be effectively smaller by a factor of about 2 at these wavelengths. Another potential cause for the loss in sensitivity is related to signal-to-noise ratio (S/N) in different bands viewed at the stage of optical fiber transmission. As already mentioned, spectral dependence of the amplifier gains and cable losses together causes significant gradient in the signal level across our wide-band, although we have tried to reduce it as much as possible. Due to constraints on the total RF power level to be input to the fiber transmission unit (after allowing for due headroom for RFI), the contrast in spectral density of our signal to that of the transmitter noise gets seriously compromized in bands where signal level is relatively low (resulting from gain-slopes). Improvement in sensitivity at the higher bands would necessarily require addressing both these issues, with suitable modifications in the feed design as well as employing multiple fibers to carry different sections (2 to 3) of the wide band separately to avoid degradation of S/N. While these are being pursued, efforts are also going on to miniaturize the whole receiver, significantly reducing its physical size for ease of portability.

For completeness, we mention infrequent but noticeable occurrences of data-slips, caused by occasional slowness in capturing of the high-rate stream of packets to the disk, in the present data (such gaps in data sequence are apparent in Figure 9; note the randomly distributed dark vertical lines across various bands). This issue has now been resolved by using a software tool "Gulp" (Corey 2007) which provides a significantly larger buffer between packet-capturing from the ethernet and disk-writing, enabling lossless capture of packets at high rates.

Although the development of the MBR is primarily motivated by the tomographic studies of pulsar polar emission regions and would aid probe of several aspects of pulsar emission

at single-pulse resolution, the potential of simultaneous multi-frequency observations facilitated by such a system can not be overstated. In particular, while looking for fast transients, simultaneous view in multiple bands is of tremendous advantage in decisively discriminating the signals of astronomical origin from those due to RFI. While the enhancement in the formal sensitivity due to the increase in available bandwidth can be quantified trivially, the added advantage of being able to verify the consistency of a dispersed signature of any candidate event across such a wide band, though crucial, is not easily quantifiable. Apart from this, in many other multi-frequency single-dish studies where simultaneity of observations may not be crucial, usage of the MBR can help save telescope time, and the implicit compatibility in data spans, types and formats, etc, in multiple frequency bands would offer a desired ease in off-line data processing and comparisons. This capability would benefit in studying spectral evolution of the *average* properties of pulsars (e.g. pulse intensity and shapes in full Stokes), and propagation effects (including interstellar scattering/scintillation), as well as in several single-dish continuum studies (including polarization), in general. The MBR also offers a significant tunability in the center frequencies of each of the 16-MHz wide sub-bands separately, a feature advantageous particularly for surveys/studies of recombination lines.

In summary, the design and development of a self-contained multi-band receiver (MBR) reported in this paper, opens up a new powerful mode of simultaneous multi-frequency observations in 10 bands, when used with a sufficiently large aperture. The design details could be of relevance to on-going and future developments in radio astronomy instrumentation. The design and structure of the MBR is generic enough to enable its use at any suitably large single-aperture telescope. The preliminary results, from the initial observations carried out using our MBR system at the GBT, provide a glimpse of the exciting phase ahead in such pulsar emission tomographic studies we intend to carry out in greater detail.

Facilities: GMRT, GBT

REFERENCES

Backer, D. C. 1973, ApJ, 182, 245

Corey Satten 2007, Lossless Gigabit Remote Packet Capture With Linux, http://staff.washington.edu/corey/gulp/

Deshpande, A. A. & Rankin, J. M. 1999, ApJ, 524, 1008

Deshpande, A. A. & Rankin, J. M. 2001, MNRAS, 322, 438

Drake, F. D. & Craft H. D. E. 1968, Nature, 220, 231

Maan, Y., Amiri, S., Raja, W. & Mehta, N. 2009, ASP Conference Series, 407, 430

Olsson, R., Kildal, P. S. & Weinreb, S. 1981, IEEE Trans. Ant. Prop., 54, 2

Radhakrishnan, V. & Cooke, D. J. 1969, Astrophys. Lett., 3, 325

Rankin, J. M. 1983, ApJ, 274, 333

Ramachandran, R., Deshpande, A. A. & Indrani, C., 1998, A&A, 339, 787

This preprint was prepared with the AAS LaTeX macros v5.2.
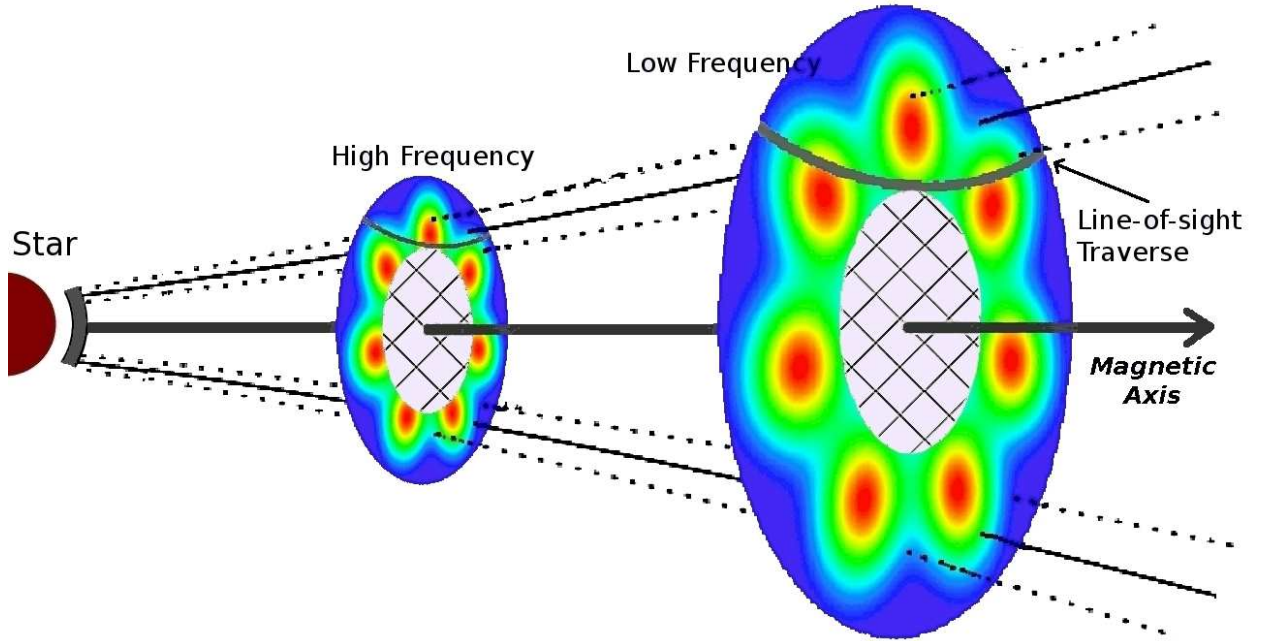
Fig. 1.— A cartoon to illustrate tomography of polar emission region, wherein two of the many possible slices of the emission cone are shown consistent with the radius-to-frequency mapping. The gray arcs indicate the line-of-sight traverse. Given the single pulse time sequences, 2-D pictures similar to those shown in the example slices, can in principle be mapped using a cartographic transform (for details, see Deshpande & Rankin 2001). The size of the inner inaccessible region (cross-hatched) is determined by how close our sight-line gets to the magnetic axis.
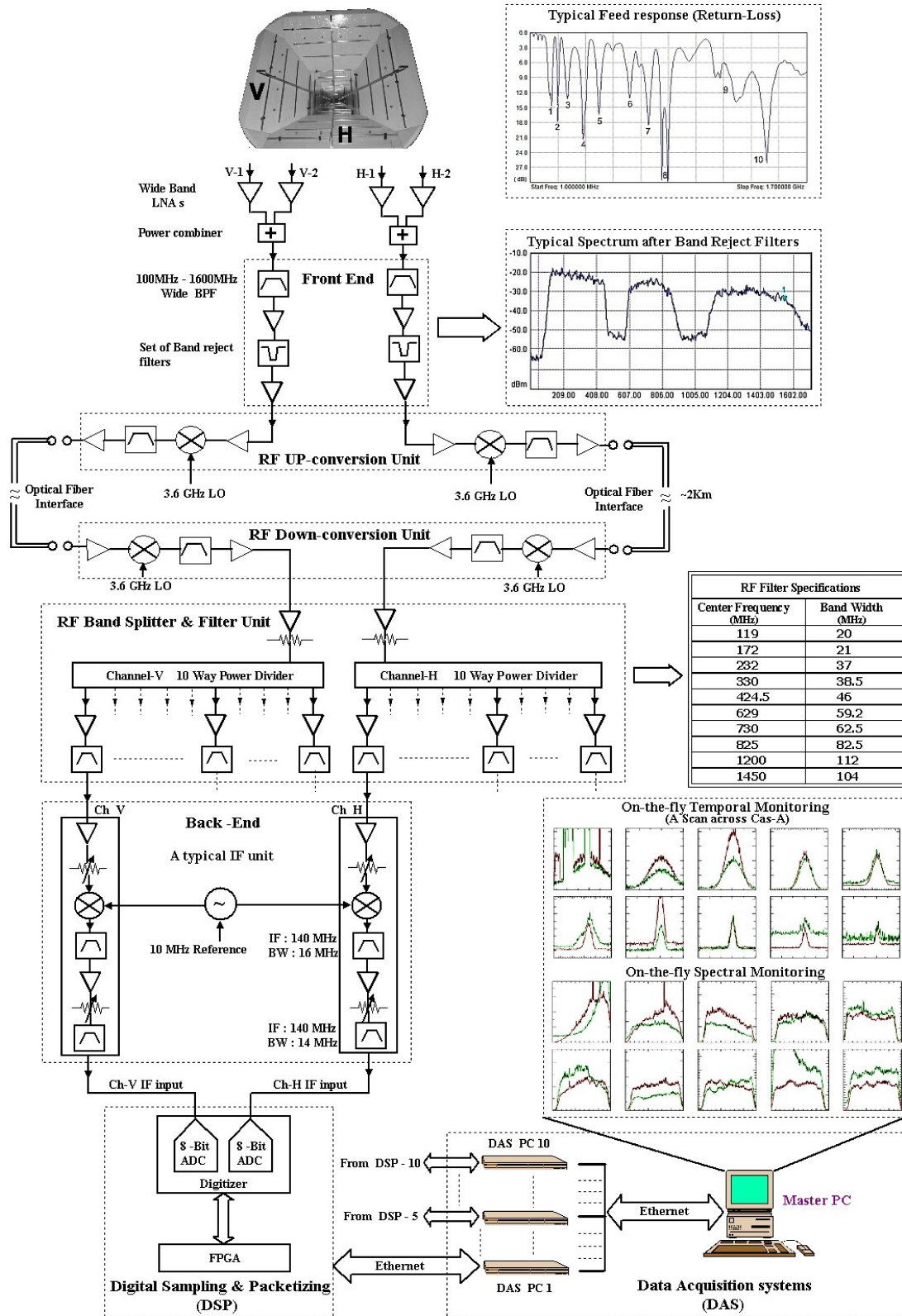
Fig. 2.— The overall block diagram of the MBR.
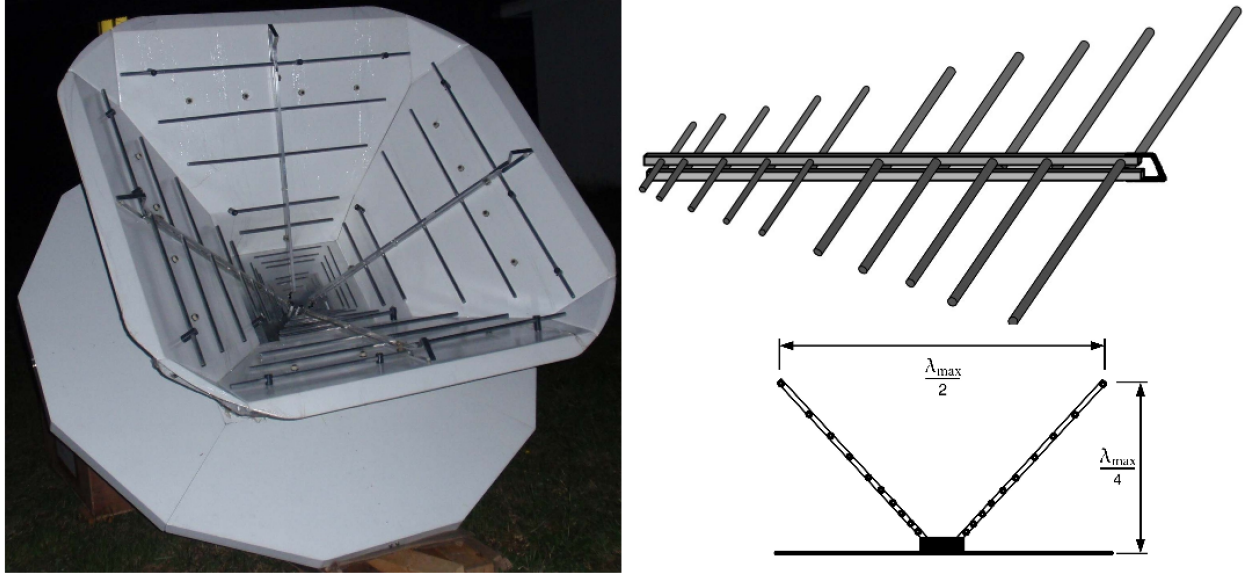
Fig. 3.— Multi-Band Feed Schematics; Left: A photograph of the multi-band feed installed at the primary focus of the GBT. Right: Upper part shows the position arrangement of dipoles for one half of the single polarization feed, lower part shows the lateral view of the single polarization feed-element.
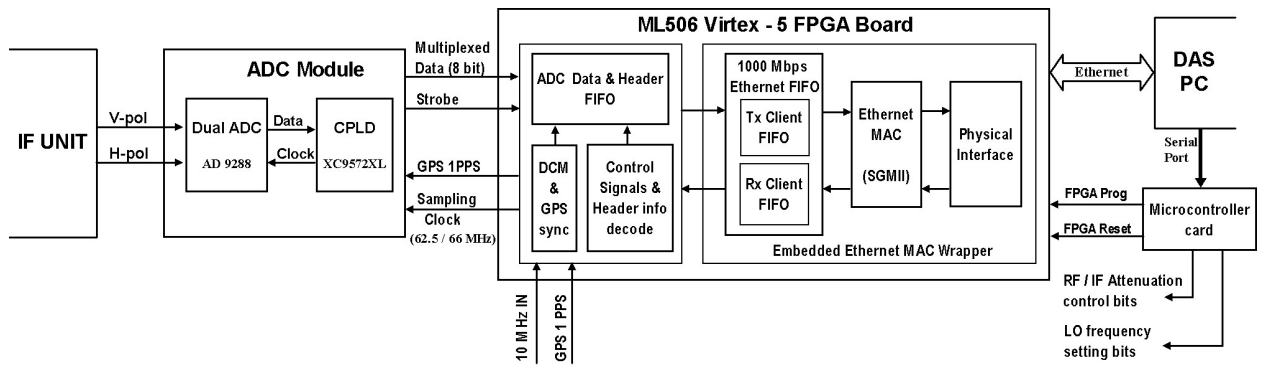
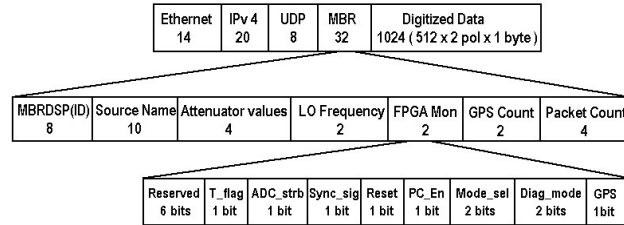Fig. 4.— Block diagram of the "Digital Section" in a typical sub-band receiver chain.

Fig. 5.— Ethernet Data Packet Structure (The numbers shown in the first two rows are in terms of bytes, as opposed to bits in the third row).
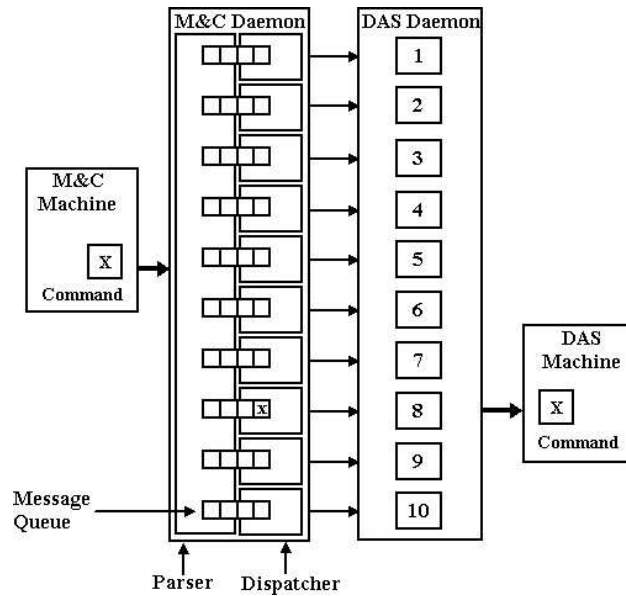
Fig. 6.— Software architecture of the MBR system. Here, 'X' is a command intended for DAS 8. The parser unit of the M&C daemon pushes this command into the message queue for the eighth dispatcher, which in turn sends the command over the network to the DAS daemon. The DAS daemon runs the binary corresponding to the command.
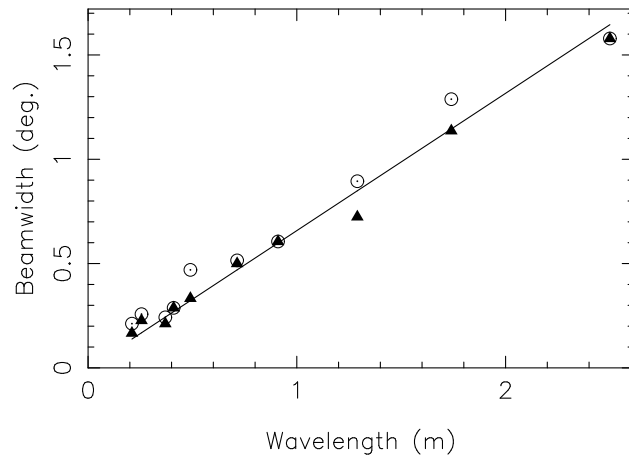
Fig. 7.— Estimated beam-widths from Cas-A scans are examined for linear dependence on wavelength (corresponding to the center frequencies listed in Figure 2). The circles & triangles correspond to the estimates for the beams associated with the two orthogonal linear polarizations. The solid line indicates the best-fit linear trend modelling the wavelength dependence of the observed beam-widths.
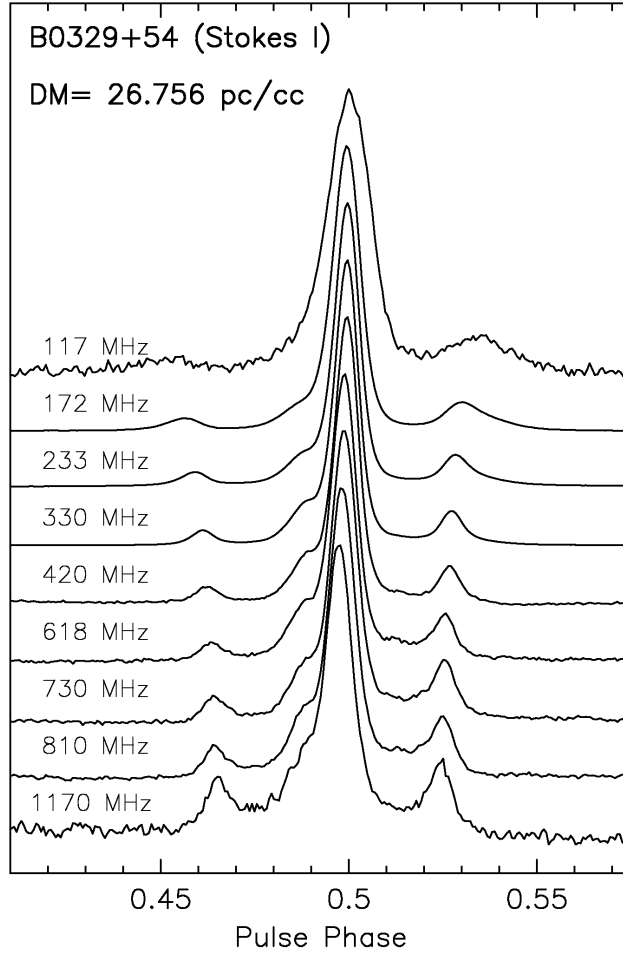
Fig. 8.— The average profiles of the bright pulsar B0329+54 obtained from simultaneous observations in the 9 bands, after appropriate dedispersion, show spectral evolution of the pulse profile in total intensity.
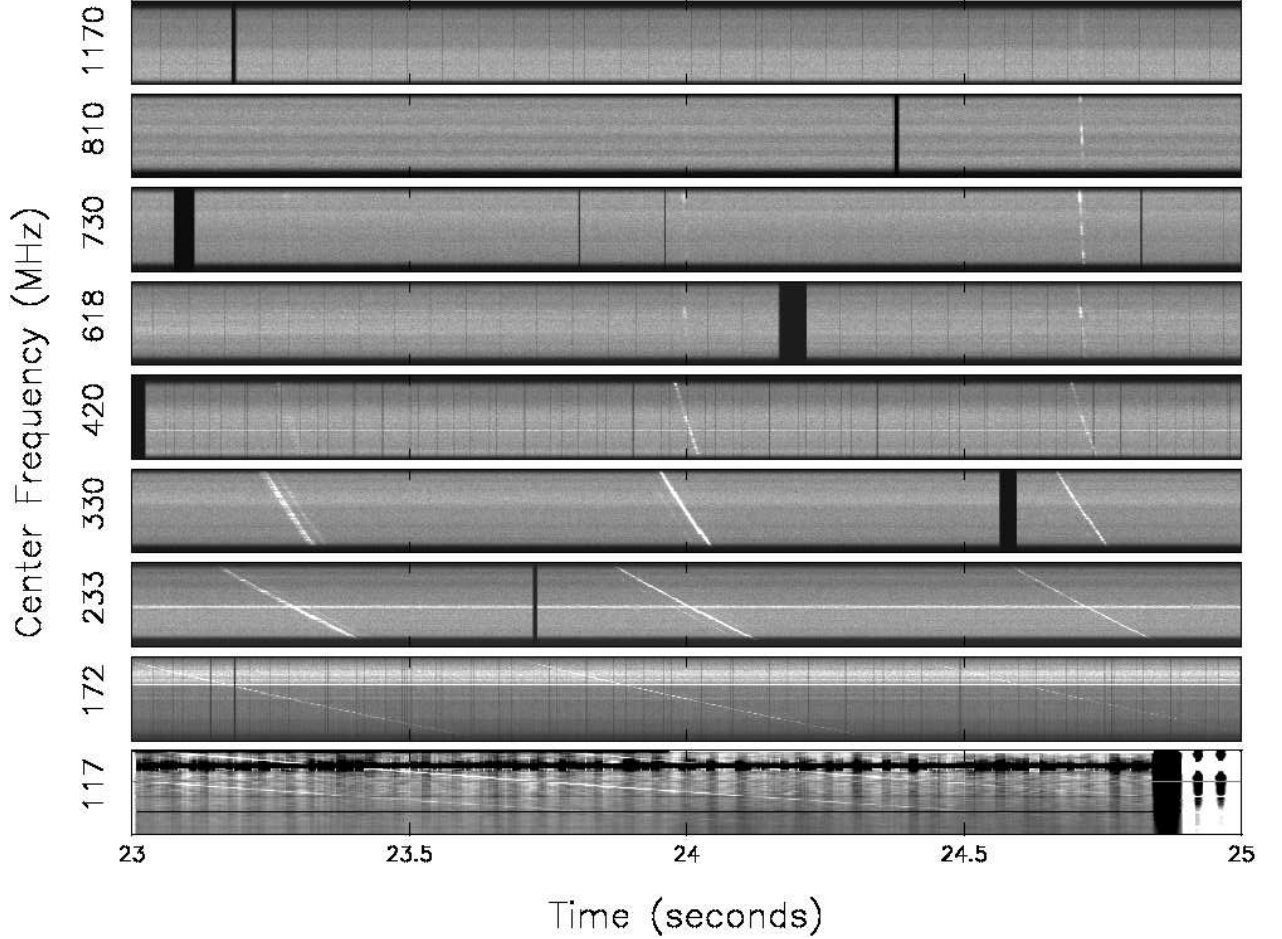
Fig. 9.— The dynamic spectra for each of the 9 bands (stacked together), across a 2-seconds span, are shown here. The faint slanted & curved streaks within the bands highlight the dispersed pulses, wherein the data across the various bands have been shifted, removing the relative dispersion delays between the respective bands (referenced to respective center frequencies). As expected, the slope of the streaks becomes shallow as we go to lower frequency bands with steep increase in the dispersion delays across the respective bands. The first band (centered at 117 MHz) is severely contaminated by strong wide-band (e.g. white patch between $\sim 24.9 - 25$ seconds) as well as narrow-band RFI.
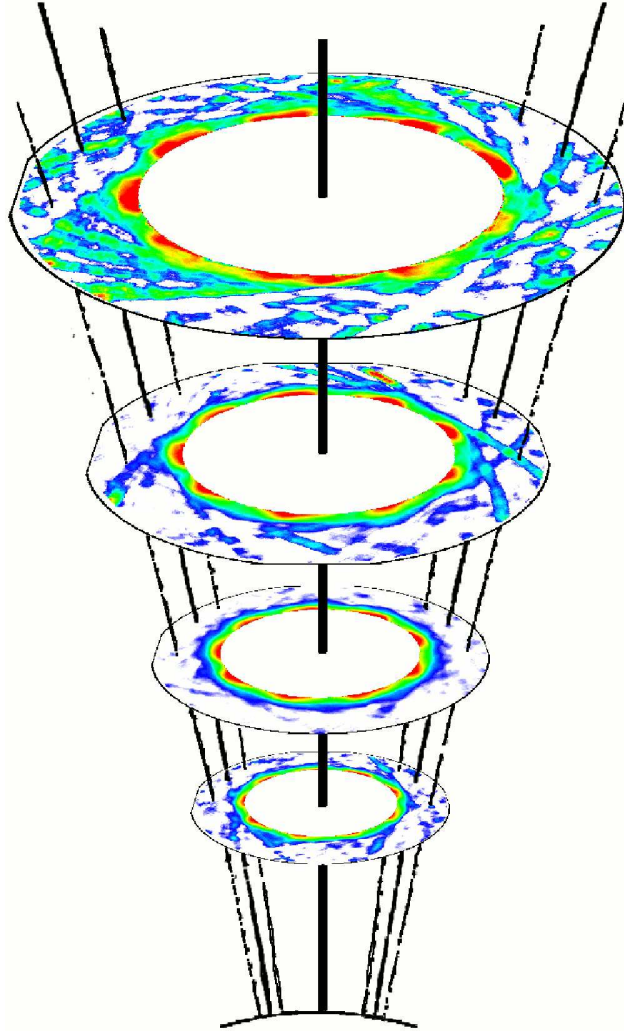
Fig. 10.— This preliminary tomographic view of the polar emission region of the pulsar B0809+74 is obtained by vertically stacking maps of the underlying emission patterns at the 4 lowest frequency bands (across 117-330 MHz), where each map is resulted from cartographically transforming the single pulse fluctuations observed at the corresponding radio frequency. The relative locations and sizes of these patterns, chosen conveniently, are consistent with the essential qualitative trends of radius-to-frequency mapping and geometry of the emission cone. The overall similarity of the patterns across frequency, in terms of the number of sub-beams (the high intensity regions corresponding to the red color) and their relative locations, is clearly evident. The partial sampling of the radial extent of the sub-beam is seen to improve systematically towards lower frequencies, corresponding to the expected broadening of the polar emission cone.